

Phase coherence in multiple scattering : weak and intense monochromatic light wave propagating in a cold strontium cloud

David Wilkowski, Yannick Bidel, Thierry Chanelière, Robin Kaiser, Bruce Klappauf and Christian Miniatura

Institut non linéaire de Nice, UMR 6618 du CNRS, 1361 route de Lucioles, F-06560 Valbonne, France.

May 24, 2005

ABSTRACT

For large bulk disordered media, light transport is generally successfully described by a diffusion process. This picture assumes that any interference is washed out under configuration average. However, it is now known that, under certain circumstances, some interference effects survive the disorder average and in turn lead to wave localizations effects. In this paper, we investigate coherence of a monochromatic laser light propagating in an optically thick sample of laser-cooled strontium atoms. For this purpose, we use the coherent backscattering effect as an interferometric tool. At low laser probe beam intensities, phase coherence is fully preserved and the interference contrast is maximal. At higher intensities, saturation effects start to set in and the interference contrast is reduced.

1. INTRODUCTION

One of the fascinating properties of photons, like all quantum objects, is interference. In the well-known two-slits experiment, the photon experiences the two slits at the same time, *i.e.* takes two different paths to reach the detector. The detection probability P is obtained from the superposition principle which states that $P = |A_1 \exp(i\varphi_1) + A_2 \exp(i\varphi_2)|^2$ where $A_n \exp(i\varphi_n)$ is the quantum mechanical amplitude to go through slit n while the other is closed. Interference effects are then encoded in the phase-difference $\varphi = \varphi_2 - \varphi_1$. As a result, depending on the φ value, the two paths may interfere constructively or destructively and correspondingly lead to an increased or decreased detection probability and thus to interference fringes. These quantum interferences are very sensitive to any phase-breaking mechanisms destroying coherence.

The same principles apply for monochromatic light shining and being scattered off an optically thick disordered sample. For a given configuration of scatterers, the scattered light exhibit a well-known speckle pattern. This pattern originates from the coherent superposition of all possible quantum amplitudes $A_p \exp(i\varphi_p)$ associated to each possible scattering path p inside the medium. The detection probability is thus now $P = |\sum_p A_p \exp(i\varphi_p)|^2$. Averaging now over all possible scatterers configurations, one may think that all interference terms of the form $\sum_{p \neq q} A_p A_q \exp(i(\varphi_p - \varphi_q))$ will be washed out. This is true *unless* paths p and q are *geometrically the same but travelled in opposite direction*. We then say that we face pairs of *reversed* paths. In this case, disorder average cannot break the *two-wave* interference associated to these pairs of scattering paths. This is the basic surviving interference effect at the heart of the coherent backscattering (CBS) phenomenon. Collecting light retro-reflected off the sample, the average detection signal exhibits a narrow angular cone around exact backscattering. The angular width of the CBS cone typically scales as $(k\ell)^{-1}$ where k is the light wave vector and ℓ the light scattering mean free path inside the sample. This CBS cone is a hallmark of interference effects in multiple scattering¹⁻³ even if other interference effects which survive disorder-average also exist : weak localization effects (interference corrections to the Boltzmann diffusion constant), universal conductance fluctuations,^{2, 4, 5} *etc.*

Technically speaking, the semi-classical picture developed so far to explain interference effects in multiple scattering is valid in the (weak localization) regime $k\ell \gg 1$. When disorder is so strong that the onset $k\ell \approx 1$ is reached (Ioffe-Regel criterion), then a disorder-induced "metal-insulator" transition occurs. Optical states

in the bulk are exponentially localized and transport is inhibited. This is the celebrated Anderson scenario (strong localization phenomenon) valid for any kind of linear waves.^{6,7} For infra-red optical light, only one experimental observation⁸ has been reported so far but further investigation is still required due to possible residual absorption.^{9,10}

The CBS effect can be used as a powerful interferometric tool to study possible phase-breaking mechanisms at work while the light wave interacts with a random medium. As a (multi) two-wave interferometer, the CBS interferometer shares many similarities with other, more common, two-wave interferometers like the two-slit set-up. However it has also some particular and unusual properties: it is an automatically self-aligned, zero path-length set-up. This interferometer is thus very robust. The CBS enhancement factor α , defined as the ratio between the intensity collected at exact backscattering and the intensity collected far off exact backscattering, is a measure of the degree of coherence of light leaving the medium. When coherence is fully preserved, α takes its maximal value in the so-called parallel polarization channels and is exactly 2 for spherically symmetric scatterers in the helicity-preserving polarization channel $h\parallel h$. In this case, any phase-breaking mechanism inducing a coherence loss between the interfering multiple scattering reversed paths is expected to yield an enhancement factor smaller than 2 in the $h\parallel h$ channel.

This makes the CBS interferometer an unique tool to study decoherence effects in multiple scattering. As an example, we may cite the decoherence induced by a Zeeman-degenerate internal structure (for experiment see^{11,12} and¹³ for theory) and also the corresponding surprising restoration of interference by applying an external magnetic field.¹⁴

In this paper we present a collection of CBS experiments done with a cold strontium (⁸⁸Sr) atomic cloud as an optically thick disordered medium. Using an atomic gas to investigate wave transport phenomena offers substantial advantages with respect to classical Mie or Rayleigh scatterers. First, as point-dipole scatterers, the maximum light scattering cross-section $\sigma = 6\pi/k^2$ is far much larger than the square of the geometrical size itself. Scattering is thus very efficient. Second, as atoms are extremely resonant scatterers, a slight detuning of the incoming light with respect to the internal atomic resonance (by few linewidths Γ) can change by several orders of magnitude the light scattering efficiency. Third, atoms of a given species are perfect monodisperse scatterers. The major drawback is the large transport time $\tau^* \gtrsim \Gamma^{-1}$ ($\approx 5 ns$ for strontium)¹⁵ which imposes a Doppler broadening much smaller than Γ .¹⁶ Cooling atoms in a Magneto-Optical Trap (MOT) circumvents this difficulty.

The strontium MOT and its main characteristics will be given in section 2. Then in section 3, we will describe the results obtained in two different regimes : the elastic scattering regime obtained at low laser intensities and the inelastic scattering regime obtained at high laser intensities. In the first case, coherence is fully preserved while in the second case it is altered due to vacuum-induced dipole fluctuations.

2. COLD ATOMIC CLOUD

2.1. MOT set-up

The cold strontium cloud is produced in a magneto-optical trap (MOT) set-up. The cooling transition is the optical dipole transition line $^1S_0 - ^1P_1$ at $\lambda = 461 nm$. This transition thus connects a $J_g = 0$ ground state to a $J_e = 1$ excited state. The excited-state natural linewidth is $\Gamma/2\pi = 32 MHz$ and the corresponding saturation intensity is $I_s = 42.5 mW/cm^2$.

First an effusive strontium beam is extracted from an oven operating at $500^\circ C$. Then a $27 cm$ long Zeeman slower reduces the strontium longitudinal velocity within the velocity capture range of the MOT, *i.e.* $\sim 50 m/s$ (Fig. 1a). The Zeeman slower, MOT, and probe laser beams all operate at $461 nm$ and are generated from the same frequency-doubled source detailed in.¹⁷ Briefly, a single-mode grating stabilized diode laser and a tapered amplifier are used in a master-slave configuration to produce $500 mW$ of light at $922 nm$. This infrared light is then frequency-doubled in a semi-monolithic standing-wave cavity with an intra-cavity $KNbO_3$ nonlinear crystal. The cavity is maintained at resonance with the infrared light thanks to a feedback loop. The second harmonic exits the cavity through a dichroic mirror providing $150 mW$ of tunable single-mode light, which is then frequency locked on the $461 nm$ strontium line in a heat pipe (Fig. 1b). We use acousto-optic modulators for subsequent amplitude and frequency variations. The MOT is made of six independent trapping beams. Each

beam is carrying an intensity of 5.2 mW/cm^2 and each beam waist is 8 mm . The trapping beams are red-detuned by $\delta = -\Gamma$ with respect to the atomic resonance line. Two anti-Helmholtz coils generate a 70 G/cm magnetic field gradient to trap the atoms.

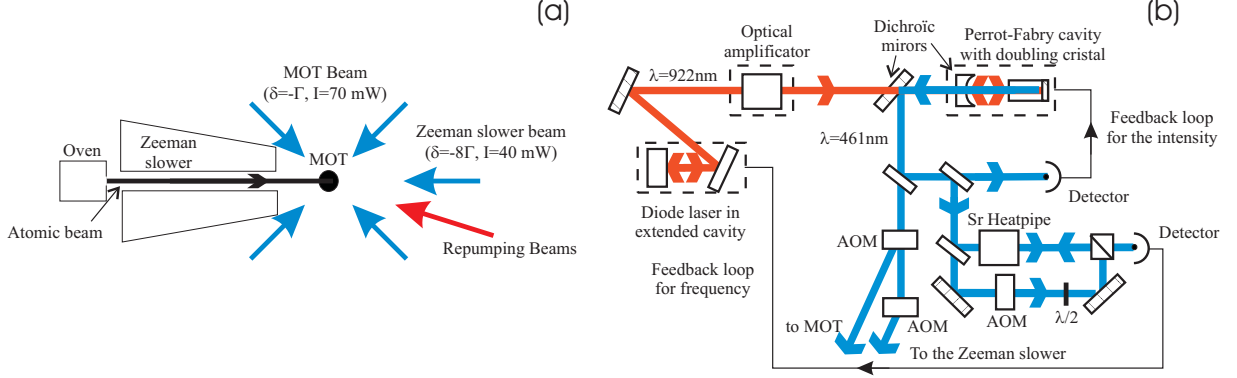


Figure 1. MOT (a) and Laser (b) set-ups . For more details see text.

2.2. MOT parameters

2.2.1. Trapped population

The 461 nm transition used for cooling is not a closed transition. Hence, atoms in the 1P_1 state can radiatively decay to the 1D_2 state and then to the triplet 3P_1 and 3P_2 states (see Fig. 2). Atoms ending in the long-lived 3P_2 state are then lost. The maximum optical pumping loss rate (obtained at large laser intensities) is 410 s^{-1} whereas the loading atomic flux in our experiment is about 10^9 s^{-1} . Hence pumping losses can reduce the number of trapped atoms down to typically 10^6 atoms but do not prevent by themselves the formation of the cold atomic cloud. In Fig. 3, the MOT lifetime is shown as a function of the saturation parameter s

$$s = \frac{s_0}{1 + 4\delta^2/\Gamma^2} \quad (1)$$

where $s_0 = I/I_s$ is the on-resonance saturation parameter (I being the total MOT laser intensity) and δ is the laser detuning. The plain curve is obtained by considering optical pumping as the only loss mechanism with no adjustable parameters. We see that the overall experimental behavior is well reproduced by this simple model. We think that the small mismatch may come from systematic errors in the measurements of the laser intensity or detuning.

In principle, atoms should be efficiently shielded from these optical pumping losses by adding two additional lasers on resonance with the $^3P_2 \rightarrow ^3S_1$ line at 707 nm and with the $^3P_2 \rightarrow ^3S_1$ line at 679 nm . Using only the 707 nm laser, atoms are pumped to the 3P_0 metastable state. The relative maximum gain G of the trapped population should then be:

$$G = \frac{\Gamma_{^3S_1 \rightarrow ^3P_1}}{\Gamma_{^3S_1 \rightarrow ^3P_0}} \quad (2)$$

It corresponds to the ratio between the inverse decay probability of the 3S_1 state to the 3P_0 and the inverse decay probability of the 3S_1 state to the 3P_1 state. From Fig. 2, we get $G = 3$. Hence the maximum gain of the trapped population should be $1 + G = 4$. However the measured gain is only around 2.5, *i.e.* lower than the expected value. We think that this discrepancy is due to the MOT magnetic field gradient which expels the atoms pumped in the anti-trapping Zeeman states of the 1D_2 and 3P_2 levels.

By using the two pumping lasers, the number of trapped atoms is increased up to about $N \approx 10^8$. In this configuration, the MOT lifetime is essentially dominated by inelastic cold collisions, residual optical pumping and hot collisions with the uncooled strontium atoms of the atomic beam. Operating at low laser intensity, the number of trapped atoms is substantially decreased and the hot collision loss channel becomes the dominant one. In this case the MOT lifetime is found to be 0.5 s .

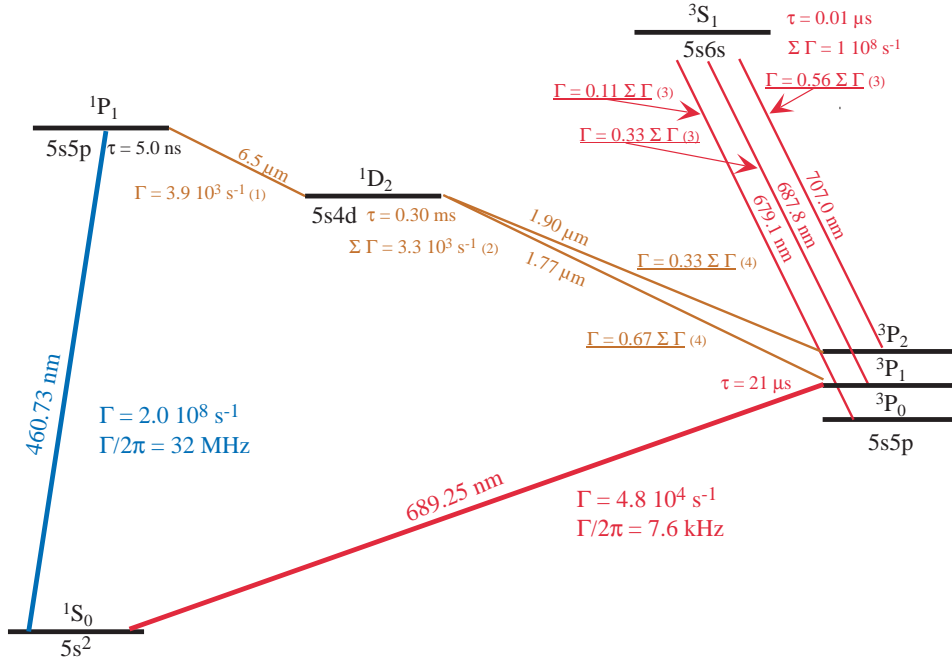


Figure 2. Energy diagram of the ^{88}Sr atom.

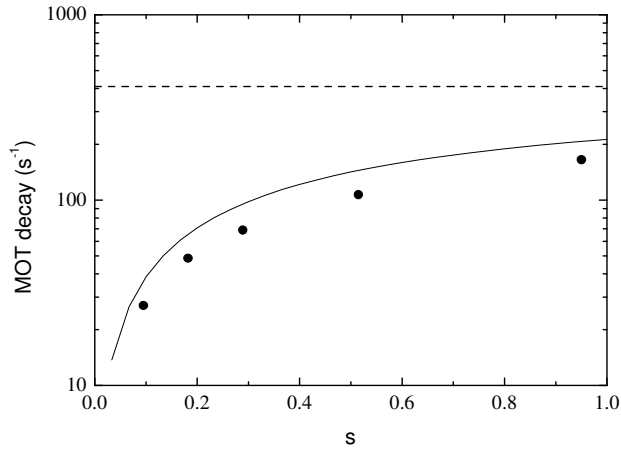


Figure 3. Measured MOT decay rate as a function of the saturation parameter s of the MOT beams (full circles) and its comparison to a theoretical model based on optical pumping losses (plain line). The dashed line corresponds to the maximum decay rate obtained at $s \gg 1$. The experiment was done at $\delta = -1.4\Gamma$.

2.2.2. Size and density

The MOT size is obtained by fluorescence imaging on a CCD camera. The MOT shape is roughly gaussian with a *rms* radius of a fraction of *mm*. In Fig. 4a, the MOT *rms* volume V is plotted as a function of the number N of trapped atoms. We have observed two different behaviors : at low laser intensities, the MOT volume is roughly independent of N while it increases with N at higher laser intensities. This phenomenon is well known¹⁸ and comes from multiple scattering of light in the cold cloud. Indeed if a scattered photon is re-scattered again in the MOT before leaving it, it induces a repulsive force between atoms and the MOT cloud inflates. If the scattering event is elastic, the repulsive force is compensated by the attractive force due to shadowing (trapping

beam attenuations). At higher intensities (see section 3.3), the scattering becomes mostly inelastic, and the repulsive force dominates. The volume of the MOT cloud is then determined by balancing the trapping and the repulsive forces. This situation is well evidenced by the plot at $s_0 = 0.45$ in Fig. 4a.

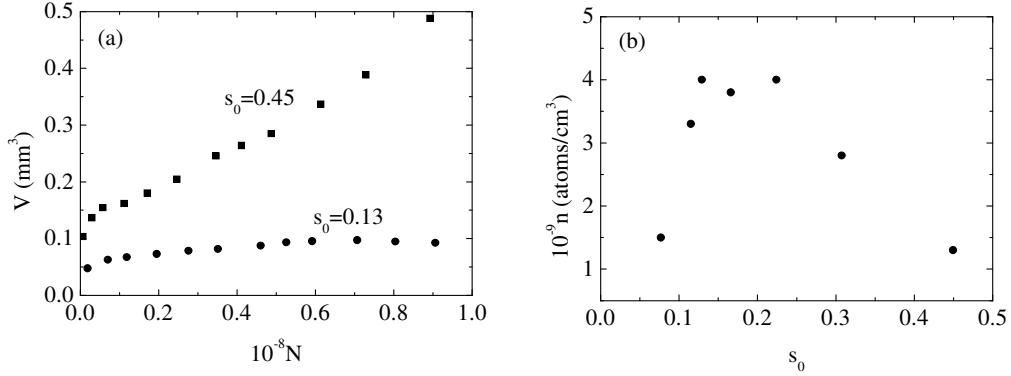


Figure 4. (a) *rms* MOT volume V as a function of the trapped population N for two different on-resonance MOT saturation parameters. When $s_0 = 0.13$, V is quasi independent of N while it increases with N when $s_0 = 0.45$. (b) MOT spatial peak density *versus* the on-resonance MOT saturation parameter s_0 . For s_0 small, N is reduced and accordingly n . For s_0 large, V increases faster than N and n is decreased. The maximum density is roughly $n \approx 4 \cdot 10^9$ atoms/ cm^3 . Both experiments were performed at $\delta = -0.9\Gamma$.

Knowing the MOT volume V and the number N of atoms, we can deduce the MOT density n . In Fig. 4b, the MOT peak density n is plotted as a function of the on-resonance saturation parameter s_0 . At low s_0 , n is reduced because the trapping force is small and N decreases. At higher s_0 , n is reduced because the multiple scattering repulsive force sets in and V is increased faster than N . The maximal density is about $n \approx 4 \cdot 10^9$ atoms/ cm^3 and is obtained at $s_0 \approx 0.15$.

2.2.3. Optical thickness

An important parameter for localization experiments is the optical thickness b of the cold cloud. This quantity is defined by the exponential attenuation of a light beam propagating through the MOT (Lambert-Beer law) :

$$I_t = I_0 e^{-b} \quad (3)$$

where I_t is the transmitted intensity and I_0 the initial intensity. Noting by L the MOT *rms* diameter, then $b = L/\ell_{ex}$ where ℓ_{ex} is known as the extinction length. When the only attenuation mechanism is depletion by scattering, the extinction length reduces to the scattering mean free path ℓ :

$$\ell = \frac{1}{n\sigma} \quad (4)$$

where n is the atomic density and σ the light scattering cross-section

$$\sigma = \frac{\sigma_0}{1 + 4\delta^2/\Gamma^2} \quad ; \quad \sigma_0 = \frac{3\lambda^2}{2\pi} \quad (5)$$

Multiple scattering is said to set in when $b \gtrsim 1$. For $b \gg 1$, light transport in the bulk is successfully described by a diffusion process. In our case, the optical depth at resonance is $b \approx 3$: it is enough to evidence multiple scattering effects but not enough to reach the diffusive transport regime. The light scattering mean free path is $\ell = L/b \approx 0.4 \text{ mm}$, giving $k\ell \approx 10^4$ ($k = 2\pi/\lambda$ is the incoming light wavevector). Our MOT cloud is thus far from achieving the Anderson localization threshold $k\ell \approx 1$ where strong localization of light is expected to occur. However, as we will see in the next sections, even in this weak localization regime where $k\ell \gg 1$, interference effects influencing transport in multiple scattering can be evidenced.

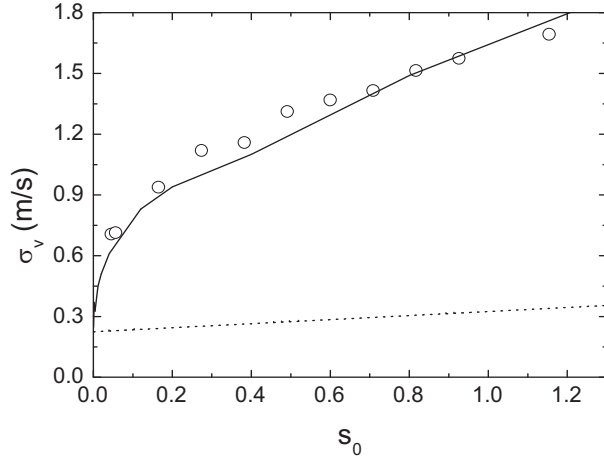


Figure 5. Measured velocity dispersion σ_v as a function of the on-resonance saturation parameter s_0 at $\delta = -\Gamma/2$. The experimental data (open circles) are compared to the bare Doppler prediction (dotted line) and to the Monte-Carlo simulation (solid line) taking into account transverse spatial intensity fluctuations. While the Doppler theory is completely off, very good agreement is found with our theoretical model (see text).

2.2.4. Temperature and phase-space density

Since the optical cooling dipole transition involves a $J_g = 0$ ground state, only Doppler cooling is present. Hence the lowest expected temperature is about 0.5 mK much higher than standard temperatures in MOTs operating with alkaline atoms where Sisyphus-type mechanisms are also present.

We have however measured here temperatures larger than the Doppler predictions. As an example, Fig. 5 shows the measured velocity dispersion σ_v in a 1D optical molasses as a function of the on-resonance saturation parameter s_0 (for more details see¹⁹). The dotted curve corresponds to the Doppler theory prediction and is completely off the experimental data. In fact, Doppler cooling proves very sensitive to heating induced by transverse spatial intensity fluctuations. The plain curve in Fig. 5 is the result of a Monte-Carlo simulation taking into account these intensity fluctuations. As one can see, a perfect agreement with experimental data is then recovered.

In the MOT, the typical measured temperature is about 5 mK ($\sigma_v \approx 1 \text{ m/s}$). Even if the situation is more complex here than in pure 1D molasses, we think that heating due to spatial intensity fluctuations still exist and explain the high temperatures found in our experiment¹⁹ but also in other earth-alkaline MOTs.²⁰⁻²³ Note however that we still have $k\sigma_v/\Gamma \approx 5\% \ll 1$ so that Doppler broadening is completely negligible.

Figure 6 displays the Strong Localization and the Bose-Einstein thresholds in the temperature and density plane. The BEC threshold occurs at a phase-space density $n\lambda_{dB}^3 \approx 2.7$. The strong localization threshold occurs at $k\ell \approx 1$ which fixes, at resonance, the density onset for localization at $n^* \approx k^3/6\pi$. For the strontium MOT operating at $\lambda = 461 \text{ nm}$, the obtained phase-space density is $n\lambda_{dB}^3 \approx 5 \cdot 10^{-12}$, thus far from the BEC onset. The achieved spatial density is $n \approx 4 \cdot 10^9 \text{ atoms/cm}^3$ still far from the density onset $n^* \approx 1.5 \cdot 10^{14} \text{ atoms/cm}^3$ at $\lambda = 461 \text{ nm}$.

3. COHERENT BACKSCATTERING

In this section we present results on CBS experiments. Section 3.2 discusses on light scattering at low saturation parameter s . In this case, the excited-state population can be ignored and the atomic dipole is successfully described by a classical damped dipole (elastically-bound electron model).²⁴ Light scattering by this classical dipole is then purely elastic. This regime is achieved either when $s_0 \ll 1$ or by sufficiently detuning the light frequency to impose $s \ll 1$.

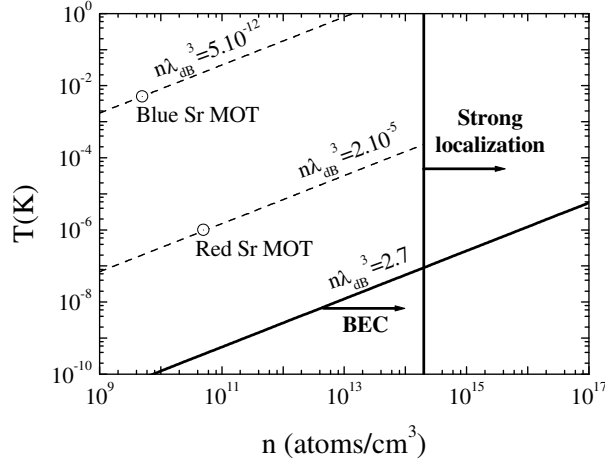


Figure 6. Strong Localization and Bose-Einstein thresholds in the temperature and density plane in Log-Log units. The BEC threshold occurs at a phase-space density $n\lambda_{dB}^3 \approx 2.7$. The strong localization threshold occurs at $k\ell \approx 1$ which fixes, at resonance, the density onset for localization at $n^* \approx k^3/6\pi$ giving $n^* \approx 210^{14}$ atoms/cm³ at $\lambda = 461$ nm. For the strontium MOT operating at $\lambda = 461$ nm, the phase-space density is $n\lambda_{dB}^3 \approx 5 \cdot 10^{-12}$. By cooling strontium atoms with the spin-forbidden transition at $\lambda = 689$ nm, the phase-space density can be increased by a factor about 10^7 while the spatial density is increased by a factor about 10. For $\lambda = 689$ nm, the density onset for strong localization is now $n \approx 4 \cdot 10^{13}$ atoms/cm³.

Section 3.3 shows the results obtained when the probe beam saturation parameter s is increased. In this case, the excited-state population is no more negligible and several related effects start to play a significant role. The first one is vacuum-induced fluctuations of the driven atomic dipole. The scattered light spectrum then exhibits a broad inelastic component giving rise to the well-known Mollow triplet at strong fields.^{25, 26} The total inelastic rate is $\Gamma_{inel} = \Gamma_{tot} s (1 + s)^{-1}$ whereas the elastic one is $\Gamma_{el} = \Gamma_{tot} (1 + s)^{-1}$ where $\Gamma_{tot} = \Gamma/2 s(1 + s)^{-1}$ is the total scattering rate (see Fig. 7). The inelastic component thus dominates over the elastic one as soon as $s > 1$. The correlation time τ_ϕ of the scattered field is then reduced down to the order of the excited-state lifetime $\tau_e = \Gamma^{-1}$. These uncontrolled field phase fluctuations during the multiple scattering events are consequently expected to yield to a decoherence mechanism. This decoherence will be effective as soon as τ_ϕ is comparable or shorter than the light transport time τ^* . For resonant scatterers like atoms, $\tau^* \geq \Gamma^{-1}$ as it is showed in¹⁵ and we see that, for inelastic scattering, $\tau^* \gtrsim \tau_\phi$. Theoretical investigations based on a simple toy-model^{27, 28} have shown that the inelastic spectrum introduces phase-shifts and amplitude imbalance between the CBS interfering paths leading to a CBS enhancement factor reduction. However, even in the limit $s \rightarrow \infty$, the CBS enhancement factor α achieves a finite value $\alpha \approx 1.05$.²⁸ This is a clear indication that decoherence induced by the inelastic spectrum is not sufficiently strong to fully erase the CBS interference effect. In the experiment, we have indeed observed a CBS reduction (see section 3.3). However, our data cannot be directly compared to the prediction of^{27, 28} who considered just two atoms alone in vacuum.

A second effect is field-induced nonlinearities. Since the excited-state population is no longer negligible, the scattering efficiency, related to the groundstate population, is reduced. This nonlinear effect is embodied in the scattering cross-section which now becomes $\sigma_{NL} = \sigma (1 + s)^{-1}$. Equivalently, the atomic susceptibility χ also shows up a dependence on the local saturation parameter s . In turn, light propagation properties are also modified : generation of a nonlinear refractive index for the effective medium (*e.g.* Kerr effect), four-wave mixing, filamentation, *etc.*²⁹ For classical scatterers, theoretical studies investigating the impact of $\chi^{(2)}$ ³⁰ and $\chi^{(3)}$ ³¹ nonlinearities do not predict any CBS enhancement factor reduction. This seems to be supported by experimental work on CBS in gain medium.³²

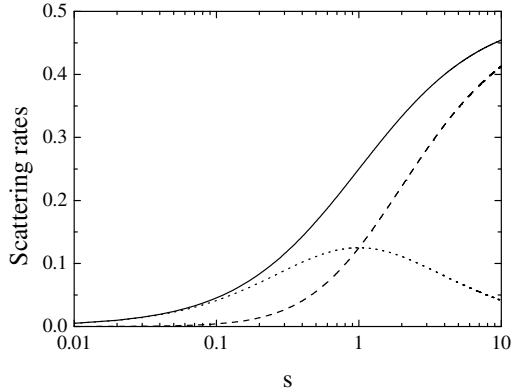


Figure 7. Light scattering rates of a two-level atom (in units of Γ) as a function of the saturation parameter s . The dotted line represents the elastic scattering rate $\Gamma_{el} = \Gamma_{tot}/(1+s)$, the dashed line the inelastic one $\Gamma_{inel} = \Gamma_{tot} s/(1+s)$. The plain line is the total scattering rate $\Gamma_{tot} = \Gamma_{el} + \Gamma_{inel} = s/2(1+s)$.

3.1. Experimental procedure and data processing

The detailed experimental procedure needed to observe light CBS on a cold atomic cloud has been published elsewhere.¹¹ For the present experiment, the signal is obtained using a collimated resonant probe laser beam with a waist of 2 mm. The scattered light is collected in the backward direction by placing a CCD camera in the focal plane of an achromatic doublet. The angular resolution of our apparatus is about 0.1 mrad , roughly twice the CCD pixel angular resolution. To shield the (weak) CBS signal from the (intense) MOT fluorescence signal, a time-sequenced experiment is developed. The MOT trapping beams and the magnetic field gradient are switched off during the CBS acquisition sequence. The probe pulse duration is adjusted accordingly (typically from 5 to $70 \mu\text{s}$) to keep the maximum number of scattered photons per atom below 400. In this way, mechanical effects can be neglected since $400 kv_{rec} \approx \Gamma/3$, where v_{rec} is the atomic recoil velocity associated with the absorption of a single photon. Once the CBS signal has been recorded, the MOT is switched on again and strontium atoms are thus recaptured. The whole sequence is then repeated as long as necessary (few minutes) to get a good CBS signal-to-noise ratio. The CBS images are finally obtained by subtracting the background image taken without any cold atoms. This background image is recorded in the absence of the magnetic gradient during all the acquisition time. We have thus checked that the fluorescence signal from the residual strontium atoms was indeed negligible.

The CBS parameters (enhancement factor and cone width) are obtained using a two dimensional fitting procedure. In the helicity polarization channels, the CBS cone is isotropic.³³ Thus the signal-to-noise ratio can be significantly improved by first pinpointing the center of the CBS cone and then performing a polar average of the image (see figures 3.1). The obtained CBS cone is then fitted by a Monte-Carlo simulation³³ performed in the elastic scattering regime and using the "partial photon" trick^{34,35} to extract the scattering contributions at different scattering orders. The amplitude of a multiple scattering path is computed as a function of the initial and final polarizations and of the geometrical positions of the various scatterers which are spatially distributed with a Gaussian of *rms* size L . The spatial variations of the scattering mean free path during the photon propagation are thus faithfully taken into account in our numerical procedure.

At low saturation parameter, the Monte-Carlo calculation is in excellent agreement with our experimental data (see Fig. 3.1a). At higher saturations, the experimental cone shape does not change significantly. Hence we still use the same Monte-Carlo calculation, performed at low saturation parameter, to fit the CBS cone even at larger s (see Fig. 3.1b).

In the fitting procedure, we have also taken into account the finite angular resolution of our detection set-up and of the residual divergence of the CBS probe laser. Thus, prior to the fitting procedure, the Monte-Carlo calculation is convolved by an appropriate Gaussian function. This allows us to remove a systematic error of about 10% on the enhancement factor value.

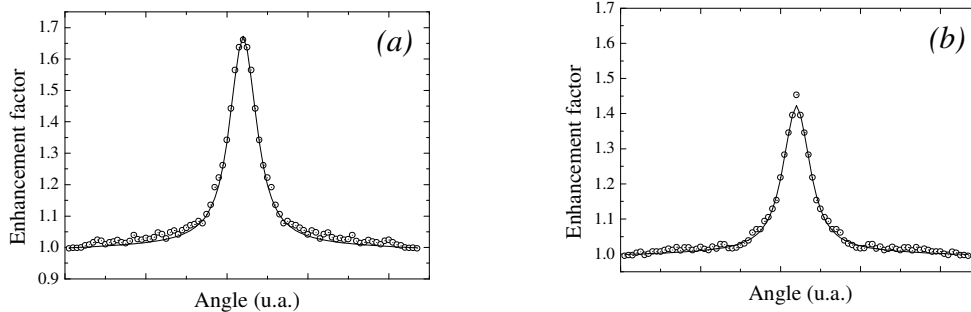


Figure 8. Plot of the experimental CBS cone as a function of the backscattering angle in the $h\parallel h$ helicity-preserving polarization channel (open circles). Both curves are obtained at $\delta = 0$. (a) $s_0 = 0.05$ (elastic regime) and (b) $s_0 = 0.71$ (saturated regime). The solid line corresponds to the Monte-Carlo simulation of the CBS cone (elastic regime) in the $h\parallel h$ polarization channel (see text).

3.2. The elastic regime

For $J_g = 0$ groundstate atoms, it can be shown that the multiple scattering interference contrast is maximal in the polarization preserving channels ($h\parallel h$ and $lin\parallel lin$ channels). This is the case for strontium. Accordingly, the enhancement factor (peak to background signal ratio) takes its maximal value 2 in the helicity preserving polarization channel $h\parallel h$ where the single scattering signal is rejected.¹³ In all other polarization channels, the enhancement factor is smaller than 2.

Using a resonant probe beam with $s_0 \ll 1$, the experimental enhancement factor is found to be $\alpha = 1.95 \pm 0.03$ at $b \approx 3$ in the helicity preserving channel ($h\parallel h$). With the same probe beam but now detuned at $\Gamma/2$ from the resonance, we found $\alpha = 1.92 \pm 0.04$ at $b \approx 1.5$. These values are very close to the maximal expected value of 2. We think that the small discrepancy is most probably due to contamination of the $h\parallel h$ polarization channel by residual single scattering signal (for more details see³⁶). This happens preferentially at low optical thicknesses where single scattering has the largest contribution to the total backscattered signal. For this reason, the enhancement factor is more reduced for $\delta = \Gamma/2$ than for $\delta = 0$. As expected, in the $h \perp h$, $lin\parallel lin$ and $lin \perp lin$ polarization channels, the enhancement factor is much smaller than 2. The results are in very good agreement with the Monte-Carlo calculations.

3.3. The saturated regime

3.3.1. Probe beam transmission

Beyond the complexity of the situation under consideration (multiple scattering with nonlinear and inelastic scatterers), one has to deal also with nonuniform scattering properties. Indeed, even in an homogeneous slab geometry, the local intensity is not constant, as the incident coherent beam is attenuated when penetrating into the medium. Hence the atoms located deeper inside the medium will not be saturated in the same way as the atoms on the front part of the sample. Thus the saturation, and hence the scattering cross-section, will not be constant along a given multiple scattering path. The importance of the spatial variation of the saturation parameter can be estimated by looking at the attenuation of the coherent beam. In Fig. 9, we report the measured transmission and we compare it with the Lambert-Beer theoretical prediction taking into account the nonlinear reduction of the cross-section. If one assumes that the local atomic saturation is dominated by the incident field and not by the scattered field, the optical transmission $T(z) = s(z)/s$, with s the incident saturation parameter, is obtained by solving the following equation:

$$(1 + sT) \frac{dT}{T} = -\frac{dz}{\ell} \quad (6)$$

The factor $(1 + sT)$ features the nonlinear reduction of the scattering efficiency. When $sT \gg 1$, $(1 + sT) \approx sT$ and $dT = -dz/s\ell$ leading to a *linear* decrease of the transmission with z

$$T(z) = 1 - \frac{z}{z^*} \quad ; \quad z^* = s\ell \quad (7)$$

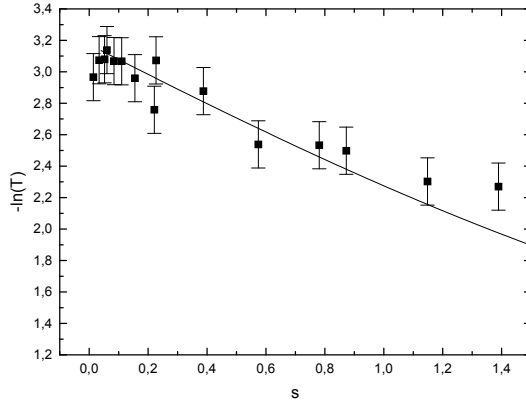


Figure 9. Resonant ($\delta = 0$) coherent transmission T along a diameter of the cold strontium cloud as a function of the incident saturation parameter s . The solid line corresponds to the theoretical nonlinear Lambert-Beer prediction (see text). The agreement with the experimental data is good up to $s = 1.2$.

When $sT \ll 1$, $(1+sT) \approx 1$ and $dT/T = -dz/\ell$ leading to the normal Lambert-Beer law and to its *exponential* attenuation

$$T(z) = \exp(-z/\ell) \quad (8)$$

Starting with $s \gg 1$, the cross-over between the two regimes $sT \gg 1$ and $sT \ll 1$ occurs around z^* . Noting by $b = L/\ell$ the low-saturation optical thickness, one immediately sees that the medium is fully saturated once $s \geq b$. For $s \leq b$, the medium can be roughly described as composed of a first saturated slice of approximate width z^* followed by a remaining non-saturated slice of width $L - z^*$.

The good agreement between the measured transmission and our simple nonlinear Lambert-Beer model (6) proves that saturation plays a role in our experimental conditions (since otherwise the transmission would not depend on s) and that the local atomic saturation is indeed dominated by the incident field.

3.3.2. Enhancement factor

Figure 10a shows the dependence of the CBS enhancement factor as a function of the incident saturation parameter s when $\delta = 0$. For each value of s , the total number of cold atoms in the cloud is adjusted in order to maintain the coherent transmission T as constant as possible ($T \approx 0.085$ in the experiment). The most striking feature is the rapid quasi-linear decrease of the enhancement factor as s is increased. The slope derived from a *rms*-procedure is $(\delta\alpha/\delta s) \approx -0.6$. The single scattering contribution has been numerically estimated to increase by less than 10% when the saturation parameter is increased up to $s = 0.8$. As the helicity-preserving polarization channel is not perfectly isolated from the single scattering signal, this increase induces a spurious reduction of the enhancement factor. We have estimated it to be of the order of 1%, thus completely negligible compared to the observed reduction. We can then faithfully claim that the observed CBS reduction comes solely from saturation effects in the multiple scattering signal.

In order to see how the atomic resonance modifies the coherence properties probed by CBS, we have performed another experiment at $\delta = \Gamma/2$. The same experimental procedure has been used with a transmission now roughly fixed at $T = 0.19$. As shown in Fig. 10b, a different general behavior is observed. First, at low intensity, the linear decreasing is faster since $(\delta\alpha/\delta s) \approx -1.8$. Second, for larger saturation parameters ($0.3 < s < 0.8$) the decrease is then slowed down. The two sets of data in Fig. 10a and 10b are obtained with a different transmission value, but other studies have shown that the enhancement factor does not sensitively depend on the exact transmission value.³⁷ Bearing this fact in mind, we are led to the conclusion that s is not the only relevant parameter in our experiment. This can be understood since the exact shape of the inelastic spectrum also depends on the detuning δ . In particular, for the detuned case, part of the inelastic spectrum will overlap the atomic resonance. This resonant inelastic light will thus be scattered again more efficiently than the off-resonant elastic part. This

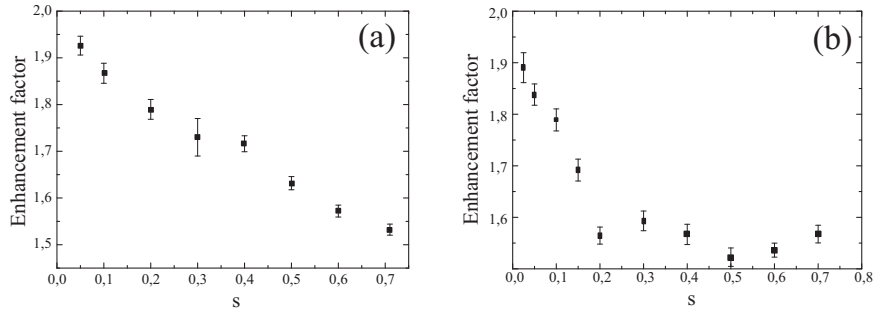


Figure 10. CBS enhancement factor as a function of the incident saturation parameter s . (a) $\delta = 0$ and (b) $\delta = \Gamma/2$. The coherent transmission value is kept fixed at $T = 0.085$ for (a) and at $T = 0.19$ for (b).

effect is *e.g.* responsible for an increase of the MOT volume in the multiple scattering regime as we discussed in section 2. Finally in our experiment, the ratio between the amount of inelastic and elastic multiply scattered light changes with the detuning. We can then conclude that the CBS reduction is due to the inelastic spectrum.

4. CONCLUSION AND PERSPECTIVES

In this paper, we have investigated phase coherence properties of a monochromatic light wave propagating in an optically thick disordered sample of laser-cooled strontium atoms. For this purpose, we have used the coherent backscattering effect as a self-aligned zero path-length interferometric tool. The CBS interference contrast is maximal when the phase coherence is fully preserved during transport and is reduced as soon as phase-breaking mechanisms set in. Concerning light scattering properties, strontium atoms behave as spherically-symmetric resonant point-dipole scatterers. We have seen that, when the incoming light is weakly saturating the atomic internal resonance, coherence is fully preserved and CBS achieves its maximal contrast 2 in the helicity-preserving polarization channel $h\parallel h$. As soon as the light intensity is increased, the CBS contrast starts to fall down indicating that phase-breaking mechanisms are at work. This is so because vacuum-induced fluctuations of the atomic dipole start to play a role. Nonlinear propagation effects as well as inelastic scattering occur which blur the CBS effect. Understanding, if not circumventing, these spurious effects is important for the quest of strong localization of light in disordered atomic samples. Indeed, localization is often explained, using hand-waving arguments, as a result of the destructive interference between long scattering paths. As such, maintaining full coherence appears as a strong request. Furthermore, a hypothetical localized optical mode in the atomic bulk may saturate atoms located in its vicinity. This phenomenon may in turn completely modify the Anderson scenario valid for linear waves. As we have seen however, our strontium MOT is far from fulfilling the density requirement to reach the strong localization onset. However subsequent cooling of ^{88}Sr on the $^1S_0 \rightarrow ^3P_1$ transition at 689 nm allows for a substantial gain in phase-space density and spatial density (see figure 6). One can even achieve phase-space densities as high as 0.1 .³⁸ One may then think to use compression techniques to reach the localization onset.

Our present studies may also prove valuable in the quest of the random laser regime in cold atoms. Coherent random lasers³⁹ are probably the most striking systems intrinsically combining both nonlinear effects and disorder. With atoms, gain and nonlinearities are easily induced. In this respect, a key point is thus a proper experimental and theoretical understanding of the mutual effects between multiple interferences and nonlinear scattering.

5. ACKNOWLEDGMENTS

The authors wish to thank D. Delande, C. Müller, T. Wellens, G. Labeyrie and J.-L. Meunier for fruitful discussions. This research is financially supported by the CNRS (Centre National de la Recherche Scientifique) and by the BNM (Bureau National de Métrologie), contract N° 03 3 005.

REFERENCES

1. E. Akkermans and G. Montambaux, *Physique mésoscopique des électrons et des photons*, EDP Sciences, France, (2004). An English translation is in preparation.
2. Mesoscopic Quantum Physics, edited by E. Akkermans, G. Montambaux, J.-L. Pichard and J. Zinn-Justin (North Holland, Amsterdam, 1995).
3. A. Akkermans et G. Montambaux, *J. Opt. Soc. Am. B* **21**, 101 (2004).
4. R. Berkovits and S. Feng, *Phys. Rep.* **238**, 135 (1994).
5. F. Scheffold and G. Maret, *Phys. Rev. Lett.* **81**, 5800 (1998).
6. "Diffuse Waves in Complex Media", NATO Science Series C, Vol. 531, Kluwer, J.P. Fouque (Ed.) (1999).
7. S. John, *Phys. Rev. Lett.* **58**, 2486 (1987).
8. D.S. Wiersma, P. Bartolini, A. Lagendijk and R. Righini, *Nature* **390**, 671-673 (1997).
9. F. Scheffold, R. Lenke, R. Tweer and G. Maret, *Nature* **398**, 206-207 (1999).
10. J. Gómez Rivas, R. Sprik, A. Lagendijk, L.D. Noordam and C.W. Rella, *Phys. Rev. E.* **63**, 046613 (2001).
11. G. Labeyrie, F. de Tomasi, J.C. Bernard, C. Müller, C.A. Miniatura and R. Kaiser, *Phys. Rev. Lett.* **83**, 5266 (1999); G. Labeyrie, C. Müller, D. Wiersma, C. Miniatura and R. Kaiser, *J. Opt. B : Quantum Semiclass. Opt.* **2**, 672 (2000).
12. D.V. Kupriyanov, I.M. Sokolov, P. Kulatunga, C.I. Sukenik and M.D. Havey *Phys. Rev. A* **67**, 013804 (2003) ; P. Kulatunga, C.I. Sukenik, S. Balik, M.D. Havey, D.V. Kupriyanov, I.M. Sokolov *Phys. Rev. A* **68**, 033816 (2003).
13. T. Jonckheere, C.A. Müller, R. Kaiser, C. Miniatura and D. Delande , *Phys. Rev. Lett.* **85**, 4269 (2000); C. Müller, T. Jonckheere, C. Miniatura and D. Delande, *Phys. Rev. A* **64**, 053804 (2001).
14. O. Sigwarth *et al.*, *Phys. Rev. Lett.* **93**, 143906 (2004).
15. G. Labeyrie, E. Vaujour, C.A. Müller, D. Delande, C. Miniatura, D. Wilkowski and R. Kaiser, *Phys. Rev. Lett.* **91**, 223904 (2003).
16. D. Wilkowski, Y. Bidet, T. Chanelière, R. Kaiser, B. Klappauf, C.A. Müller and Christian Miniatura *Phys. B* **328**, 157 (2003).
17. B. Klappauf, Y. Bidet, D. Wilkowski, T. Chanelière, R. Kaiser, *Appl. Opt.* **43** 2510 (2004).
18. D.W. Sesko, T.G. Walker and C.E. Wieman, *J. Opt. Soc. Am. B* **8**, 946-958 (1991).
19. T. Chanelière, J.-L. Meunier, R. Kaiser , C. Miniatura and D. Wilkowski, to appear in *J. Opt. Soc. Am. B.* (2005).
20. C.W. Oates, F. Bondu , and L. Hollberg, *Eur. Phys. J. D* **7**, 449 (1999).
21. F. Loo, A. Bruschi, S. Sauge, M. Allegrini, E. Arimondo, N. Andersen and J. Thomsen, *J. Opt. B: Quantum Semiclass. Opt.* **6**, 81 (2004).
22. X. Xu, T. Loftus, M. Smith, J. Hall, A. Gallagher and J. Ye, *Phys. Rev. A* **66**, 011401 (2002).
23. X. Xu, T. Loftus, J. Hall and J. Ye, "Cooling and trapping of atomic strontium ", *J. Opt. Soc. Am. B* **20**, 968-976 (2003).
24. We neglect here the recoil frequency shift which is much smaller than the linewidth $\Gamma/2\pi$.
25. C. Cohen-Tannoudji, J. Dupont-Roc, G. Grynberg, *Atom-Photon Interactions*, Wiley (1992).
26. B. Mollow, *Phys. Rev.* **188**, 1969 (1969).
27. T. Wellens , B. Gremaud, D. delande and C. Miniatura, *Phys. Rev. A* **70**, 157 (2004).
28. V. Shatokhin, C. Müller and A. Buchleitner, *Phys. Rev. Lett.* **94**, 043603 (2005).
29. R. W. Boyd, *Nonlinear Optics*, (Academic, San Diego, 1992).
30. V. Agranovich and V. Kravtsov, *Phys. Rev. B* **43** , 13691 (1991).
31. A. Heiderich, R. Maynard and B. van Tiggelen, *Opt. Comm.* **115**, 392 (1995); S.E. Skipetrov and R. Maynard *in Wave Scattering in Complex Media: from theory to applications*, NATO Science Series II **107**, eds. B.A. van Tiggelen and S.E. Skipetrov, Kluwer, Dordrecht (2003), p. 75.
32. D.S. Wiersma, M.P. van Albada and A. Lagendijk, *Phys. Rev. Lett.* **75**, 1739 (1995).
33. D. Wilkowski, Y. Bidet, T. Chanelière, D. Delande, T. Jonckheere, B. Klappauf, G. Labeyrie, Christian Miniatura, C.A. Müller, O. Sigmarth and R. Kaiser, *J. Opt. Soc. Am. B.* **21**, 183 (2004).

34. R. Lenke and G. Maret, in *Scattering in Polymeric and Colloidal Systems*, edited by W. Brown and K. Mortensen (Gordon and Breach, Reading, 2000), p. 1-72.
35. D. Delande *et al.*, Phys. Rev. A **67**, 033814 (2003).
36. Y. Bidet, B. Klappauf, J.C. Bernard, D. Delande, G. Labeyrie, C. Miniatura, D. Wilkowski, R. Kaiser, Phys. Rev. Lett. **88**, 203902 (2002).
37. Roughly speaking, inelastic scattering events occur where the saturation is high, *i.e.* in the first atomic layers. Deeper inside the medium, where saturation is low, elastic scattering events dominate. Thus varying the coherent transmission in the multiple scattering regime should not sensitively modify the inelastic mechanisms at work (and in turn the enhancement factor), at least under our experimental conditions.
38. T. Ido, Y. Isoya, and H. Katori Phys. Rev. A **61**, 061403 (2000).
39. H. Cao *et al.*, Phys. Rev. Lett. **84**, 5584 (2000); P. Sebbah and C. Vanneste, Phys. Rev. B **66**, 144202 (2002).